



Photoalignment-induced two-dimensional liquid crystal polarization structure via multi-beam polarization interferometry

YUE SHI,^{1,2} YAN JUN LIU,¹ FENG SONG,² VLADIMIR G. CHIGRINOV,³ HOI-SING KWOK,³ MINGGANG HU,⁴ DAN LUO,^{1,*} AND XIAO WEI SUN¹

¹Department of Electrical and Electronic Engineering, Southern University of Science and Technology, No. 1088, Xueyuan Rd., Xili, Nanshan District, Shenzhen, Guangdong 518055, China

²College of Physics, Jilin University, Changchun 130012, China School of Physics, Nankai University, Weijin Road 94, Tianjin 300071, China

³State Key Laboratory on Advanced Displays and Optoelectronics Technologies, Department of Electronic and Computer Engineering, The Hong Kong University of Science and Technology, Clear Water Bay, Kowloon, Hong Kong

⁴Xi'an Modern Chemistry Research Institute, Xi'an, Shanxi 710065, China

*luo.d@sustc.edu.cn

Abstract: A two-dimensional (2D) pure polarization pattern via four-beam polarization interferometry of circularly polarized beams is demonstrated both theoretically and experimentally. The polarization orientation of the interference pattern is recorded by an azobenzene photoalignment layer and transferred to liquid crystal (LC), enabling the fabrication of a 2D liquid crystal (LC) chiral structure. This structure behaves as a 2D LC polarization grating (LCPG) that can generate multiple polarization-selective diffraction beams of orthogonal polarization states with high efficiency. This 2D LCPG provides an effective way to distribute an optical signal into multiple receivers by both incidence polarization control and external electric field, therefore offering potential applications on multi-channel optical communication and information processing.

© 2018 Optical Society of America under the terms of the [OSA Open Access Publishing Agreement](#)

OCIS codes: (090.2880) Holographic interferometry; (160.1190) Anisotropic optical materials; (160.3710) Liquid crystals; (230.5440) Polarization-selective devices; (160.5335) Photosensitive materials;

References and links

1. S. Eckhardt, C. Bruzzone, D. Aastuen, and J. Ma, "3M PBS for high performance LCOS optical engine," *Proc. SPIE* **5002**, 106–110 (2003).
2. S. Yeralan, J. Gunther, D. L. Ritums, R. Cid, and M. M. Popovich, "Switchable Bragg grating devices for telecommunications applications," *Opt. Eng.* **41**(41), 1774–1779 (2002).
3. J. A. Davis, J. Adachi, C. R. Fernández-Pousa, and I. Moreno, "Polarization beam splitters using polarization diffraction gratings," *Opt. Lett.* **26**(9), 587–589 (2001).
4. J. Kim, R. K. Komanduri, K. F. Lawler, D. J. Kekas, and M. J. Escuti, "Efficient and monolithic polarization conversion system based on a polarization grating," *Appl. Opt.* **51**(20), 4852–4857 (2012).
5. L. Nikolova and T. Todorov, "Diffraction efficiency and selectivity of polarization holographic recording," *Opt. Acta (Lond.)* **31**(5), 579–588 (1984).
6. T. Huang and K. H. Wagner, "Coupled mode analysis of polarization volume hologram," *IEEE J. Quantum Electron.* **31**(2), 372–390 (1995).
7. F. Gori, "Measuring Stokes parameters by means of a polarization grating," *Opt. Lett.* **24**(9), 584–586 (1999).
8. J. Tervo and J. Turunen, "Paraxial-domain diffractive elements with 100% efficiency based on polarization gratings," *Opt. Lett.* **25**(11), 785–786 (2000).
9. M. Schadt, K. Schmitt, V. Kozinkov, and V. Chigrinov, "Surface-induced parallel alignment of liquid crystals by linearly polymerized photopolymers," *Jpn. J. Appl. Phys.* **31**(7), 2155–2164 (1992).
10. M. Hasegawa and Y. Taira, "Nematic homogeneous photo alignment by polyimide exposure to linearly polarized UV," *J. Photopolym. Sci. Technol.* **8**(2), 241–248 (1995).
11. K. Ichimura, Y. Suzuki, T. Seki, A. Hosoki, and K. Aoki, "Reversible change in alignment mode of nematic liquid crystals regulated photochemically by command surfaces modified with an azobenzene monolayer," *Langmuir* **4**(5), 1214–1216 (1988).
12. W. M. Gibbons, P. J. Shannon, S.-T. Sun, and B. J. Swetlin, "Surface-mediated alignment of nematic liquid crystals with polarized laser light," *Nature* **351**(6321), 49–50 (1991).

13. V. Chigrinov, S. Pikin, A. Verevochnikov, V. Kozenkov, M. Khazimullin, J. Ho, D. D. Huang, and H.-S. Kwok, "Diffusion model of photoaligning in azo-dye layers," *Phys. Rev. E Stat. Nonlin. Soft Matter Phys.* **69**(6), 061713 (2004).
14. G. P. Crawford, J. N. Eakin, M. D. Radcliffe, A. Callan-Jones, and R. A. Pelcovits, "Liquid-crystal diffraction gratings using polarization holography alignment techniques," *J. Appl. Phys.* **98**(12), 123102 (2005).
15. V. Presnyakov, K. Asatryan, T. Galstian, and V. Chigrinov, "Optical polarization grating induced liquid crystal micro-structure using azo-dye command layer," *Opt. Express* **14**(22), 10558–10564 (2006).
16. M. J. Escuti and W. M. Jones, "A polarization-independent liquid crystal spatial light modulator," *Proc. SPIE* **6332**, 63320M (2006).
17. C. Provenzano, P. Pagliusi, and G. Cipparrone, "Electrically tunable two-dimensional liquid crystals gratings induced by polarization holography," *Opt. Express* **15**(9), 5872–5878 (2007).
18. K. Kawai, M. Sakamoto, K. Noda, T. Sasaki, N. Kawatsuki, and H. Ono, "Tunable dichroic polarization beam splitter created by one-step holographic photoalignment using four-beam polarization interferometry," *J. Appl. Phys.* **121**(1), 013102 (2017).
19. H. Ono, A. Emoto, and N. Kawatsuki, "Anisotropic photonic grating formed in photocross-linkable polymer liquid crystals," *J. Appl. Phys.* **100**(1), 013522 (2006).
20. S. P. Gorkhali, S. G. Cloutier, and G. P. Crawford, "Two-dimensional vectorial photonic crystals formed in azo-dye-doped liquid crystals," *Opt. Lett.* **31**(22), 3336–3338 (2006).
21. U. Ruiz, C. Provenzano, P. Pagliusi, and G. Cipparrone, "Pure two-dimensional polarization patterns for holographic recording," *Opt. Lett.* **37**(3), 311–313 (2012).
22. U. Ruiz, P. Pagliusi, C. Provenzano, V. P. Shibaev, and G. Cipparrone, "Supramolecular chiral structures: smart polymer organization guided by 2D polarization light patterns," *Adv. Funct. Mater.* **22**(14), 2964–2970 (2012).
23. V. Chigrinov, H. S. Kwok, H. Takada, and H. Takatsu, "Photo-aligning by azo-dyes: physics and applications," *Liquid Crystals Today* **14**(4), 1–15 (2005).
24. Y. Shi, C. Zhao, J. Y.-L. Ho, V. V. Vashchenko, A. K. Srivastava, V. G. Chigrinov, H.-S. Kwok, F. Song, and D. Luo, "Exotic property of azobenzenesulfonic photoalignment material based on relative humidity," *Langmuir* **33**(16), 3968–3974 (2017).
25. Y. J. Liu and X. W. Sun, "Electrically tunable two-dimensional holographic photonic crystal fabricated by a single diffractive element," *Appl. Phys. Lett.* **89**(17), 171101 (2006).
26. D. Luo, X. W. Sun, H. T. Dai, Y. J. Liu, H. Z. Yang, and W. Ji, "Two-directional lasing from a dye-doped two-dimensional hexagonal photonic crystal made of holographic polymer-dispersed liquid crystals," *Appl. Phys. Lett.* **95**(15), 151115 (2009).
27. Y. J. Liu, H. T. Dai, and X. W. Sun, "Holographic fabrication of azo-dye-functionalized photonic structures," *J. Mater. Chem.* **21**(9), 2982–2986 (2011).
28. M. Born and E. Wolf, *Principles of Optics: Electromagnetic Theory of Propagation, Interference and Diffraction of Light* (Cambridge Uni. Press, 1999).
29. J. Li, J. Li, M. Hu, Z. Che, L. Mo, X. Yang, Z. An, and L. Zhang, "The effect of locations of triple bond at terphenyl skeleton on the properties of isothiocyanate liquid crystals," *Liq. Cryst.* **44**(9), 1374–1383 (2017).
30. Z. Sekkat and W. Knoll, *Photoreactive Organic Thin Films* (Academic Press, 2002).
31. L. Tan, J. Y. Ho, and H.-S. Kwok, "22:1: Binary alignment pattern induced by single step exposure of laser beam polarization interference," *SID Dig.* **43**(1), 286–288 (2012).
32. S.-T. Wu, "Birefringence dispersions of liquid crystals," *Phys. Rev. A Gen. Phys.* **33**(2), 1270–1274 (1986).
33. H. Park, E. P. J. Parrott, F. Fan, M. Lim, H. Han, V. G. Chigrinov, and E. Pickwell-MacPherson, "Evaluating liquid crystal properties for use in terahertz devices," *Opt. Express* **20**(11), 11899–11905 (2012).
34. F. Yang and J. R. Sambles, "Determination of the microwave permittivities of nematic liquid crystals using a single metallic slit technique," *Appl. Phys. Lett.* **81**(11), 2047–2049 (2002).
35. S. Stenholm, "Polarization coding of quantum information," *Opt. Commun.* **123**(1–3), 287–296 (1996).
36. Y. L. Lim, A. Beige, and L. C. Kwek, "Repeat-until-success linear optics distributed quantum computing," *Phys. Rev. Lett.* **95**(3), 030505 (2005).
37. R. L. Van Renesse, *Optical Document Security* (Artech House, 1994).
38. V. G. Chigrinov, V. M. Kozenkov, and H. S. Kwok, *Photoalignment of Liquid Crystalline Materials: Physics and Applications* (Wiley Publishing, 2008).

1. Introduction

The control of light polarization, which is of importance besides light intensity, has been utilized widely for various applications, such as polarization-based imaging systems [1], optical switching and isolating in information processing and optical communications [2]. Besides traditional polarization beam splitter, polarization grating (PG) shows great potentiality for polarization beam splitting [3] and polarization conversion [4]. The 1D PG can be obtained through interference of two coherent beams with equal intensity and orthogonal polarization states [5–7]. In particular, the interference of two orthogonally circularly polarized (CP) beams gives a uniform intensity distribution and a 1D modulated

linearly polarized (LP) light field with periodically varying polarization direction [7,8]. This polarization modulation can be recorded by polarization-sensitive materials [9–13]. Therefore, a spatially varying birefringence can be directly achieved by the photosensitive materials in volume or by a surface-aligning LC [14–16], making it a diffraction grating. By adjusting the phase retardation of the anisotropic material, the diffraction efficiency of the 0th and the 1st order can be tuned between 0% and 100% [16].

Besides 1D PG based on polarization holography [5–8,14–16], there were several reports about the 2D polarization structure, either by superposition of two 1D polarization patterns [17,18], or through multi-beam interference of LP or CP light [19–21]. However, the intensity modulations of the multi-beam polarization holography could cause either topological relief imposed 2D polarization structure of photo-sensitive polymers [19], or non-complete reorientation of the photosensitive material since null intensity areas existed in the interference field [20]. By introducing relative phases into four interferential CP beams, the intensity modulation could be suppressed, thus a 2D pure polarization microstructures was obtained [21,22]. However, the special relative phase arrangement makes it inappropriate for certain applications, and the usage of polymer makes the grating not tunable by electric field.

Here a complete investigation of the both intensity and polarization distribution are discussed for interference of four symmetrically-positioned CP beams without introducing relative phase difference. Null intensity areas could be avoided, and a chiral polarization distribution is obtained with special polarization configuration. An azobenzene small molecule is used as photoalignment layer for the polarization information recording. The anchoring strength of the thin photoalignment layer is strong enough for LC with low light exposure, and it becomes saturated with stronger illumination [23,24]. Therefore, we can avoid the problem caused by intensity modulation of the 2D multi-beam holography, and thus demonstrate a 2D pure polarization microstructure based on interference of four symmetrically-positioned CP beams without relative phase. This method makes it easier to adapt to integrated optics such as fiber lasers and optical prisms [25–27]. Based on this method, a 2D polarization structure with intrinsic chiral property, i.e. a 2D chiral photonic crystal, can be obtained by photoaligned LC or LC polymer. This 2D polarization structure performs as a 2D LCPG that processes multiple CP diffraction beams in the 1st order with orthogonal polarization states and high efficiency, and the diffraction is polarization selective. Therefore, it provides an effective approach to distribute an optical signal into multiple receivers by polarization control of the incidence light, and the diffraction efficiency can be adjusted by external electric field. Both simulation analysis and experimental results are discussed in this paper, giving a complete investigation of the 2D polarization structure and grating property.

2. Simulation and Experimental

The four-beam polarization interference setup is built based on a 488 nm Ar⁺ laser with long coherence length on a floated optical table. The laser beam splits into two first, and then each beam splits into another two symmetrically [Fig. 1(a)]. In this symmetric optical configuration, no phase difference exists between each other. A pair of polarizer and quarter-wave plate (QWP) is put in each arm to generate CP light, and a half-wave plate (HWP) is put before polarizer for light intensity control. The four beams converge symmetrically along the orthogonal planes with the same polar angle θ , which is chosen to be 3.5° for both simulation and experiment. The interference polarization distribution is recorded by a photosensitive sample at the interference plane, and the intensity distribution can be monitored by a charge-coupled device (CCD) camera with proper optical magnification.

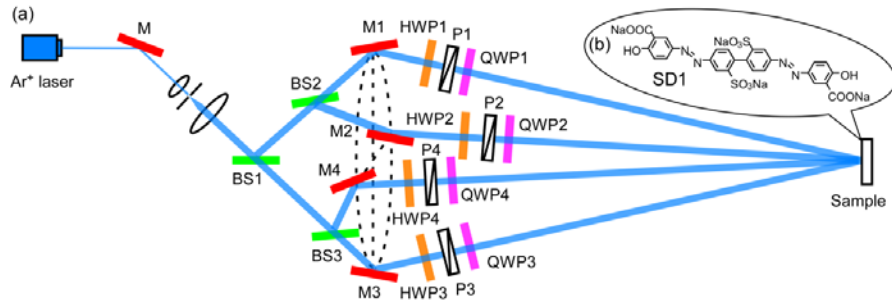


Fig. 1. (a) Schematic setup of the four-beam polarization interferometry. M: mirror; BS: beam splitter, P: polarizer. (b) Chemical structure of azobenzene photoalignment material SD1.

The light interference can be simulated through Matlab[®]. $\vec{E}_i = A\hat{p}_i \exp\{i\vec{k}_i \cdot \vec{r}\}$ is the electric field of each beam with the same intensity, A is the amplitude and \hat{p}_i is the polarization vector with $\hat{p}_{LCP} = (1, i)^T / \sqrt{2}$ for left circularly polarized (LCP) light and $\hat{p}_{RCP} = (1, -i)^T / \sqrt{2}$ for right circularly polarized (RCP) light respectively. The propagation vectors of the four symmetric beams are $\vec{k}_1 = k[\sin\theta, 0]$, $\vec{k}_2 = k[-\sin\theta, 0]$, $\vec{k}_3 = k[0, -\sin\theta]$, and $\vec{k}_4 = k[0, \sin\theta]$, where $k = 2\pi/\lambda$. The z -component is neglected and only the interference pattern on the x - y plane will be discussed. The sum of the vector fields of the four beams is $\vec{E}(x, y) = \sum_{i=1}^4 \vec{E}_i(x, y)$, and the intensity distribution is $I(x, y) = |\vec{E}(x, y)|^2$. To explore the polarization state, the electric field of interference can be expressed as $\vec{E}(x, y) = (A_x e^{i\delta_x}, A_y e^{i\delta_y})^T$, which is elliptically polarized (EP) in general and can be fully characterized by its ellipticity, orientation angle and helicity [28]. An auxiliary parameter γ is introduced as the ratio of the y - to x -component, $\gamma = A_y e^{i\delta_y} / A_x e^{i\delta_x} = A_{yx} e^{i\delta}$. The orientation angle ψ is calculated as $\tan 2\psi = 2\text{Re}[\gamma] / (1 - |\gamma|^2)$. The ellipticity is the minor to major axis ratio of the polarization ellipse $\mp b/a = \tan \chi$, where χ is the ellipticity angle determined by $\sin 2\chi = -2\text{Im}[\gamma] / (1 + |\gamma|^2)$. The helicity of the ellipse is indicated either by angle χ or δ . The angle χ is in the range of $[-\pi/4, \pi/4]$, and δ can be adjusted to the range of $[-\pi, \pi]$. If $0 < \chi \leq \pi/4$ or $0 < \delta < \pi$, it is right-handed polarized. If $-\pi/4 \leq \chi < 0$ or $-\pi < \delta < 0$, it is left-handed polarized. When $\chi = 0$, the EP light degenerates to LP, and when $\chi = \pm\pi/4$, it is CP light.

An azobenzene sulfonic dye SD1 (DIC Inc.) is used as the photoalignment material for the interference pattern recording [Fig. 1(b)] [22,23]. To get a photoalignment layer, the SD1 powder is dissolved in N,N-dimethylformamide (DMF) at a concentration of 1 wt% and spin-coated on glass substrate at 3000 rpm for 30 s, which is then soft-baked at 100 °C for 10 min for solvent evaporation, giving a 10 nm-thick solid film. After exposure to the interference pattern with 80 mW/cm² recording intensity for 5 min, the polarization orientation is recorded by the photoalignment layer. A layer of LC polymer UCL017 (DIC Inc., $\Delta n = 0.17$) is then spin-coated on top, whose thickness can be adjusted to achieve desired phase retardation value. The LC directors will follow the director distribution of SD1 molecules due to the anisotropic anchoring effect, and an additional deep UV polymerization process fixes the LC director distribution to make it a solid microstructure without disturbing the patterned alignment. The 2D LC pattern can be visualized under polarized optical microscopy (POM). The local transmitted light intensity of LC between crossed polarizers is

$I = I_0 \sin^2(2\varphi) \sin^2(\pi\Delta nd / \lambda)$, where Δnd is the LC phase retardation and φ is the director azimuthal angle.

A 457 nm solid state laser is used as probe beam to investigate the diffraction property of the 2D polarization microstructure. The probe beam is LP, which could change to LCP or RCP by going through a QWP with its fast axis $+45^\circ$ or -45° to the polarization direction. The polarization of the diffracted light by the LCPG is checked by a rotating polarizer, and the helicity of the CP light is checked by going through a QWP and a polarizer with the polarization axis $+45^\circ$ or -45° to the fast axis of the QWP based on Jones calculus. For simulation, the grating diffraction can be obtained by Fourier transform of the transmitted electric field through the LCPG $\vec{E}_{out}(x, y) = T(x, y)\vec{E}_{in}$. $T(x, y)$ is the transfer matrix of a wave plate T_{WP} with spatially varying director field $\varphi(x, y)$, $T(x, y) = R[-\varphi(x, y)]T_{WP}R[\varphi(x, y)]$, where $R[\varphi(x, y)]$ is the rotation matrix.

On the other hand, a 2 μm -thick ITO glass cell with SD1 inter coating on both substrates is also exposed to the interference pattern with the same illumination condition, and then a nematic LC material HM2 with high birefringence $\Delta n = 0.37$ [29] is filled into the patterned cell by capillary action. A 632.8 nm He-Ne laser is used as probe beam to investigate the diffraction property of the tunable grating to avoid pattern erasing, and a sinusoidal ac voltage is applied to the cell to adjust the LC phase retardation.

3. Results and Discussion

For interference of four symmetric CP beams with the same intensity and no relative phase difference, there are four different combinations of CP light helicities as listed in Table 1 and shown in Fig. 2(a). Other CP light combinations give similar results with only pattern rotation, flipping or polarization reversion. In contrast to the two CP beam interference whose intensity is constant [5,6,14–16], the intensity distribution of the four CP beam interference is not uniform in our configuration [Figs. 2(b) and 2(c)]. In case 1, the intensity maxima are located on a 2D square lattice with periodicity $\sqrt{2}\Lambda$, where $\Lambda = \lambda / 2 \sin \theta$. In case 2, the maximum intensity areas get elongated in the x -direction. In case 3, the intensity distribution is a 2D square lattice with periodicity Λ . In case 4, the intensity distribution becomes 1D stripes oriented at 45° . The intensity maximum (I_{max}) and minimum (I_{min}) of different cases are listed in Table 1. In case 1, 3 and 4, the intensity minimums are zero, while $I_{min} = A^2$ in case 2 and thus no null intensity areas exist in the interference field. Figure 2(c) shows the experimental intensity distributions, consistent with the simulation results.

Table 1. Comparison of Four Symmetric CP Beam Interference with Different Polarization Configurations^a

| Case | Configuration | I_{min}/I_{max} | Polarization | Polarization Orientation |
|------|-----------------|-------------------|--------------|--------------------------|
| 1 | RCP-RCP-RCP-RCP | $0/16A^2$ | CP | / |
| 2 | RCP-RCP-LCP-RCP | $A^2/10A^2$ | EP | continuous |
| 3 | RCP-LCP-RCP-LCP | $0/8A^2$ | EP | 90° jump |
| 4 | LCP-LCP-RCP-RCP | $0/8A^2$ | LP | continuous |

^a A^2 is the light intensity of one of the four interference beam.

Besides intensity, the polarization distribution of the interference field is of particular interest [Fig. 2(d)]. In case 1, there is no polarization modulation, which is the same as incidence. Contrarily, modulated LP light with periodically varying polarization direction as the 2-beam PG is obtained in case 4, with a 45° rotation and $\sqrt{2}\Lambda$ as the periodicity. For the other two cases, the interference electric field is EP where the ellipticity and orientation are position-dependent. In case 3, the orientations of the polarization ellipses are either 0° or 90° in the adjacent squares with periodicity Λ . The 90° orientation jump is realized by gradually changing ellipticity. In case 2, however, both the ellipticity and orientation of the ellipse change continuously and gradually with position.

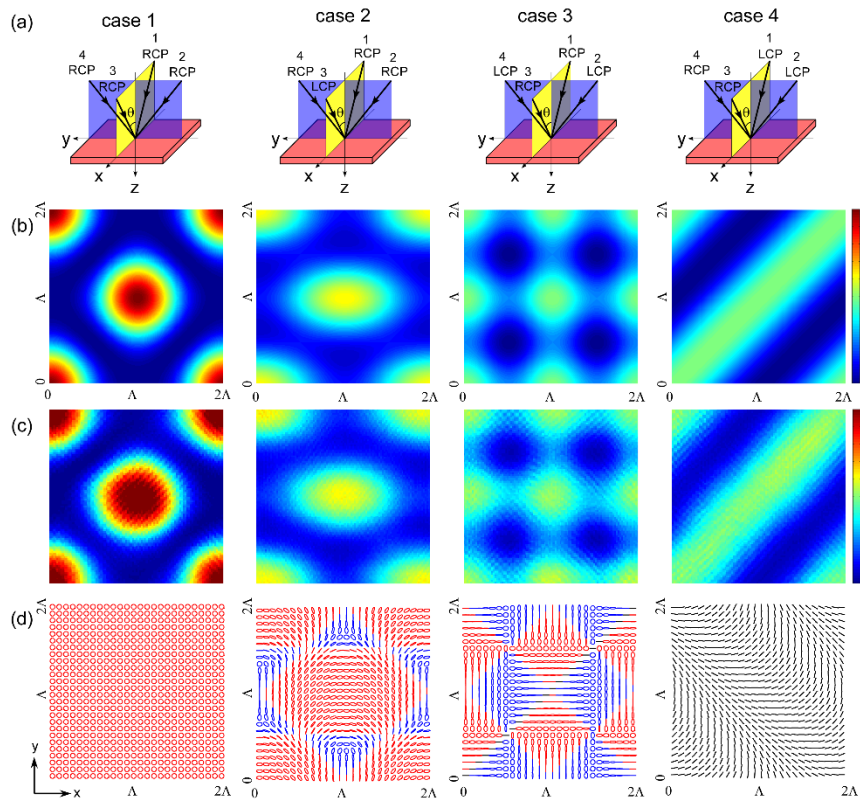


Fig. 2. Interference of four symmetric CP beams with different polarization configurations. (a) Schematic diagrams of the four-beam arrangement. (b) Simulated intensity distribution of the interference pattern. (c) Experimental intensity distribution. (d) Simulated polarization distribution of the interference field. Different colors indicate different polarization states. Blue: left-handed polarization; Red: right-handed polarization; Black: linear polarization.

As known, when exposed to LP light, the azobenzene molecules align perpendicularly to the polarization direction [30]. If the excitation light is EP, azobenzene molecules will then align perpendicularly to the long axis of polarization ellipse with strong enough exposure dosage [31]. Based on the discussion above, case 2 is suitable for photoalignment of LC, since the orientation of polarization ellipse varies continuously in the x - y plane and the intensity distribution has no null area. Therefore, the polarization orientation can be fully recorded by the azobenzene photoalignment material in this case. We use a thin layer of SD1 azobenzene material for the polarization pattern recording (“case 2” omitted). Average exposure dosage of 24 J/cm^2 is used to ensure that strong anchoring can be induced even at the minimum intensity area (6 J/cm^2) while the alignment of maximum intensity areas (60 J/cm^2) gets saturated [22,23]. Then a layer of LC polymer is spin-coated on top and then UV cured to obtain a uniform solid film with periodically varying director field. The LC textures from both simulation and experiment are shown in Figs. 3(a) and 3(b) under POM. The LC directors are perpendicular to the long axis of the polarization ellipse, which is visualized in Fig. 3(c) corresponding to Fig. 2(d) in case 2. A periodic 2D pure polarization structure with intrinsic chiral property, i.e. a 2D chiral photonic crystal, is thus obtained by photoaligned LC.

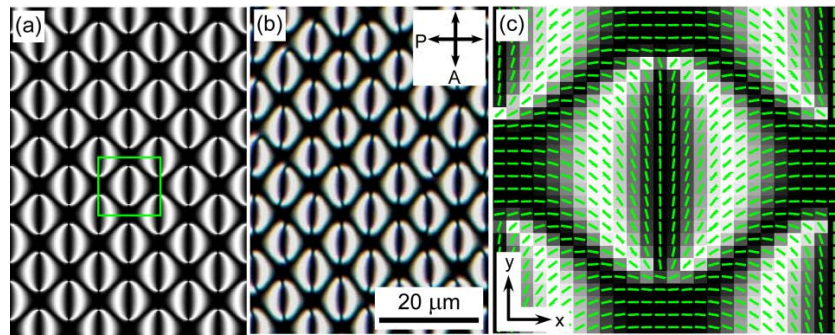


Fig. 3. 2D LC chiral texture observed under POM (case 2). (a) Simulated LC texture. (b) LC texture realized experimentally. (c) Simulated LC texture with director configuration (green short lines) in one period.

The periodic 2D chiral structure could diffract light as PG. The diffraction has several diffraction orders, as shown in Fig. 4. The 0th order is in the center, keeping the original propagating path. The 1st order consists of six diffraction spots with equal intensity, which occupies most of the diffraction energy. The 2nd order possesses 4 diffraction spots, which are much dimmer around the 1st order. There are even higher orders that can be neglected due to extremely low diffraction efficiency. Figures 4(a)-4(c) show that the diffraction efficiency η varies with LC phase retardation, and the detailed dependence of the first three orders is plotted in Fig. 4(d). The maximum diffraction happens at half-wave condition ($\Delta nd = \lambda/2$), where the 1st order occupies about 85% of the total energy. These properties are valid at least from UV to microwave range, as long as the LC material keeps anisotropic and not absorbent [32–34].

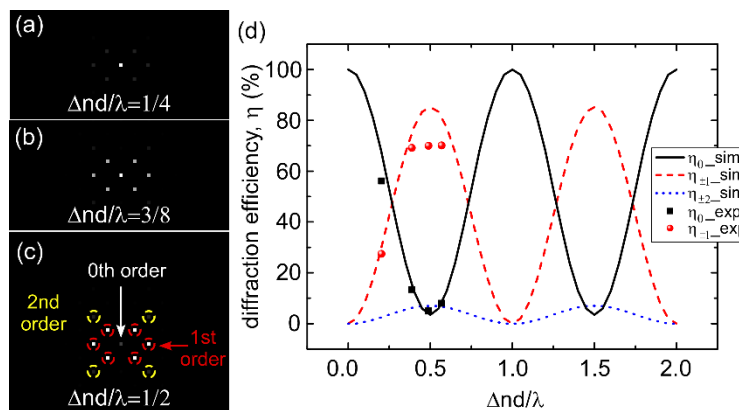


Fig. 4. Diffraction of the 2D LCPG with different LC phase retardation based on simulation (case 2). (a)-(c) Diffraction intensity distribution. The 0th, 1st and 2nd orders are marked respectively in (c). (d) Diffraction efficiencies of the 0th, 1st and 2nd orders from both simulation and experiments.

The diffraction of the 2D LCPG is expected to be polarization sensitive due to its chiral property. The simulation result shows that the unpolarized or LP light can be diffracted into all the orders [Fig. 5(a)], while CP light is mainly diffracted into the positive or negative orders depending on its helicity [Figs. 5(b) and 5(c)]. There is very weak energy leakage of the diffracted light to the other side, which can be barely seen in Figs. 5(b) and 5(c). The leaked power of the 1st order is about 1.27% of the main opposite ones (contrast ratio ~ 79) from simulation based on Fourier transform. The light polarization can be monitored by the phase difference δ_{diff} between the y - and x -component of the diffracted electric vector, which keeps unchanged regardless of phase retardation [Figs. 5(d) and 5(e)]. With CP incident light,

the diffraction is pure CP with opposite helicity to the incidence, where RCP has $\delta_{diff} = -\pi/2$ and LCP has $\delta_{diff} = \pi/2$. If the incident light is LP, which can be split into a pair of LCP and RCP light, the 1st order diffractions are the superposition of that from LCP and RCP light. Therefore, the diffraction of LP light is nearly CP due to the weak diffraction leakage, which is indicated by the small difference of δ_{diff} compared to $\pm \pi/2$ as shown in the inset of Fig. 5(e). The small energy leakage is probably because that the 2D LCPG is constructed by photoalignment technology, which can only record the polarization orientation, and thus the complete recovery of the interference field is not obtained. However, the leaked energy is low enough to be neglected in practical application.

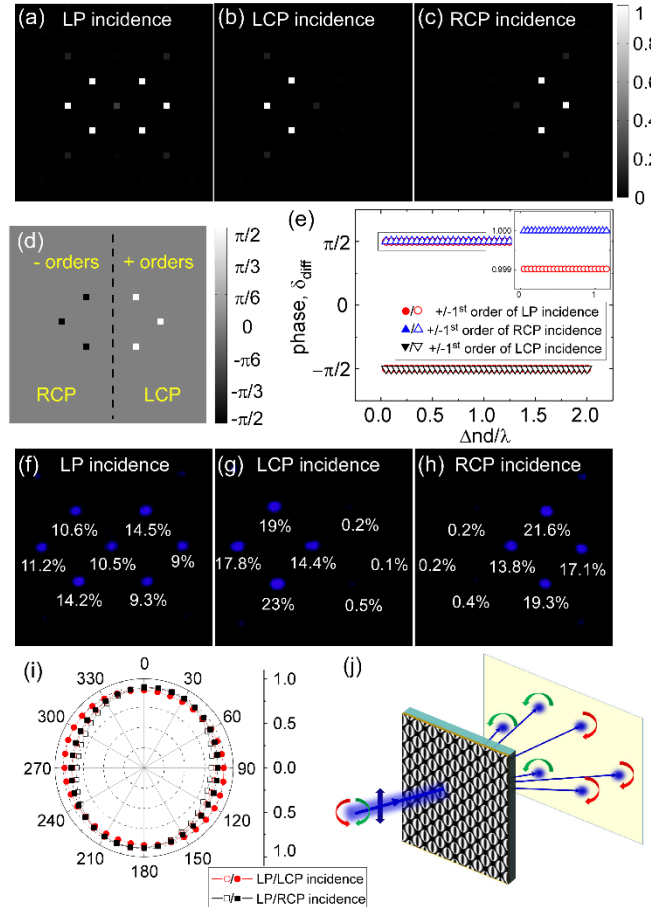


Fig. 5. Polarization investigation of the 2D LCPG diffraction (case 2). (a)-(c) Simulated diffraction intensity with different polarization incidence at half-wave condition. (d) and (e) The simulated phase δ_{diff} of the main 1st order beams. Inset: normalized δ_{diff} of diffractions from CP and LP light. (f)-(h) Experimental diffraction with different polarization incidence on the 2D LCPG ($d \sim 1.3 \mu\text{m}$). The diffraction efficiencies are measured and marked in the figure. (i) Polarization measurements (normalized intensity vs. polarizer angle) of the 1st order of LP (open symbols) and CP incidence (closed symbols) respectively from experiments. (j) Schematic illustration of the 2D LCPG diffraction with different incident polarization.

To confirm the simulation result, the diffraction of the 2D LCPG is investigated experimentally [Figs. 5(f)-5(i)]. The helicity of the diffracted light can be checked by going through a QWP and a polarizer at $\pm 45^\circ$ based on Jones calculus. Upon 457 nm laser incidence, the LCP light is mainly diffracted into the three -1 st orders on the left which are RCP [Fig. 5(g)], and the RCP incident light is mainly diffracted into the three $+1$ st orders on

the right that are LCP [Fig. 5(h)]. The leaked 1st order light on the opposite side is small compared to the main ones from experiment as marked in the figure. For LP light incidence, the six main 1st order diffraction spots are observed [Fig. 5(f)]. The polarization of the diffracted light is checked by a rotating polarizer, as shown in Fig. 5(i), indicating the diffracted beams are near CP. The diffracted light ellipticity with LP light incident is smaller (0.82/0.88 for LCP/RCP diffracted light respectively) compared to that of CP incidence (0.94/0.94 for LCP/RCP diffracted light respectively) due to the energy leakage, which are basically consistent with the simulation results. But the measured light ellipticity is actually smaller than expected, and the measured diffraction efficiencies of the 1st order are also lower than the simulation result [Fig. 4(d)]. The maximum diffraction efficiency $\eta_{\pm 1}$ is found to be ~70% of the total power from experiment, which is lower than the expected value of 85%. Although the imperfect incident CP probing light and the scattering from LC polymer could lower the diffraction efficiency and cause the imperfect CP diffracted light, the discrepancies are mainly due to optical misalignment of the multi-beam interference setup. Simulation shows that a small misalignment of one beam in the interference setup will cause the diffraction efficiency drop significantly, for example, a 0.35° misalignment lowers the 1st order diffraction to 73%, and the misalignment also lowers the ellipticity of diffracted light with LP incidence (results not shown). This small misalignment is hard to be completely avoided in our experiments by hand adjustment. However, integrated optical systems using fiber lasers or optical prisms could improve the results [24–26]. The polarization selective multi-channel diffraction property of the 2D LCPGs, as schematically illustrated in Fig. 5(j), shows great potentiality for applications in optical communications [2], quantum computing [35,36] and optical security industries [37]. In addition, the complex PG structures may be extended to nano-scale with larger interferential polar angle, providing an effective way for chiral photonic crystal/quasicrystal fabrications.

On the other hand, if a nematic LC is filled into a four-beam interference patterned cell instead of using LC polymer, an electrically switchable 2D LCPG could be constructed. The LC effective birefringence Δn_{eff} can be controlled continuously by applied ac voltage, and thus the diffraction efficiency η is adjustable. Here, a nematic LC with high birefringence is used to allow wide adjustable range in a thin cell. The electro-optical behavior of a 2D LCPG is shown in Fig. 6. The diffraction efficiency of the 1st order $\eta_{\pm 1}$ at off state is low since the effective phase retardation ($\Delta n_{eff}d$) is near λ . As voltage increases, Δn_{eff} decreases. When $\Delta n_{eff}d$ reaches $\lambda/2$, $\eta_{\pm 1}$ is maximum and η_0 is minimum. Then $\eta_{\pm 1}$ decreases with voltage until Δn_{eff} approaching to 0, where the diffraction is mainly to the 0th order. Here $\eta_{\pm 1}$ is lower than that of LC polymer film on one photo-patterned substrate. This is firstly due to the undefined pretilt angle of LC, which causes defects and thus decreases the diffraction efficiency with applied voltage. Secondly, there is small difference of the interference pattern at the front and back substrates of the cell due to the cell gap. The two mismatched patterns cause the binary grating effect, and therefore lead to higher order diffractions and the non-vanishing 0th order at half wave condition. This effect becomes more serious if the cell gap gets thicker [15]. However, these problems could be further optimized, for example, by using smaller interference polar angle and smaller cell gap, or by introducing uniform pretilt angle after pattern recording [38].

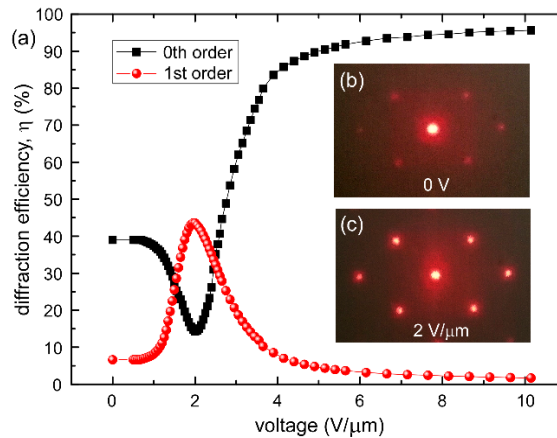


Fig. 6. Diffraction of the 2D LCPG as a function of applied electric field ($f = 1\text{kHz}$). (a) Diffraction efficiencies of the 0th and 1st order as a function of applied electric field. (b) and (c) Diffraction patterns at different voltages respectively. A uniformly aligned nematic LC cell is used as 100% efficiency reference. All given voltages are peak to peak values.

4. Conclusion

In conclusion, a 2D pure polarization structure with intrinsic chiral property has been demonstrated through a four-CP-beam interferometry. The four CP beams are symmetrically arranged without relative phase difference between each other. The interference with different polarization configurations is discussed, where an EP electric field with periodically changing polarization orientation without intensity null is chosen to induce anisotropic anchoring of the azobenzene photoalignment layer, and then transferred to LCs. The resulting 2D LCPG has multiple diffraction spots in the 1st order with high efficiency. The diffraction is polarization selective and the diffracted beams have orthogonal CP polarization states, providing an effective way to distribute an optical signal into multiple channels by polarization control of the incident light. On the other hand, the multi-beam interference with any polarization configuration can be predicted based on the simulation method, and different polarization structures could be realized experimentally through multi-beam polarization interference based on photoalignment technology.

Funding

This work is supported by National Natural Science Foundation of China (NSFC) (61405088, and 11674183); Shenzhen Science and Technology Innovation Council (JCYJ 20160226192528793, and KQTD2015071710313656); National Key Research and Development Program of China administrated by the Ministry of Science and Technology of China (2016YFB0401702), and Foshan Innovation Project (2014IT100072).